ACS Catalysis

Letter

pubs.acs.org/acscatalysis

High Performance Pt Monolayer Catalysts Produced via Core-Catalyzed Coating in Ethanol

Yu Zhang,[†] Yu-Chi Hsieh,[†] Vyacheslav Volkov,[‡] Dong Su,[§] Wei An,[†] Rui Si,[†,⊥] Yimei Zhu,[‡] Ping Liu,[†] Jia X. Wang,*[,†] and Radoslav R. Adzic*[,†]

[†]Chemistry Department, [‡]Condensed Matter Physics & Materials Science Department, [§]Center for Functional Nanomaterials, Brookhaven National Laboratory, Upton, New York 11973, United States

Supporting Information

ABSTRACT: Platinum monolayer core−shell nanocatalysts were shown to have excellent catalytic activities and stabilities. Usually, they are fabricated via electrochemical routes. Here, we report a surfactant-free, ethanol-based, wet chemical approach to coating Pd nanoparticles with uniform Pt atomic layers, inspired by aerobic alcohol oxidation catalyzed by the Pd cores. The as-prepared Pt monolayer electrocatalysts also exhibited high electrocatalytic performance toward the oxygen reduction reaction.

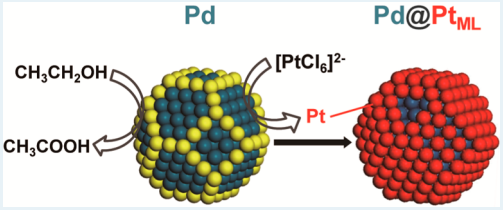

KEYWORDS: *core shell, atomic layer coating, platinum monolayer, electrocatalysis, nanostructure, oxygen reduction, catalyst*

Platinum (Pt) is a catalyst of paramount importance for many reactions,[1−3] such as the oxygen reduction reaction (ORR) in fuel cells and batteries.[4] However, the high price and limited reserves of Pt have posed a challenge of enhancing Pt utilization in Pt-based catalysts.[5,6] Recently, the Pt content has been greatly reduced via core−shell nanostructures consisting of a Pt shell on appropriate monometallic or alloy cores.[7,8] Especially, the highest Pt utilization along with enhanced activities and durability have been achieved in the Pt monolayer (Pt_{ML}) nanocatalysts with a one-atom-thick Pt shell,[9−11] where every Pt atom is on the catalysts' surface and available for participating in electrocatalytic reactions.

The Pt monolayer deposition on various core nanoparticles has been primarily accomplished in an electrochemical route using galvanic displacement by Pt of Cu[12−15] or other metal[16−18] monolayers formed by underpotential deposition (UPD). Alternatively, the adsorption/absorption of gas molecules such as hydrogen[19−22] or carbon monoxide[23] can be controlled to a suitable amount for Pt_{ML} deposition. The combination of both methods is operative, as well.[24] These two methods can eliminate the multiple layer growth of Pt by having a limited amount of reducing agent right on the core particles' surface. However, compared with the significant success with assistance of a reductant layer of metal atoms or gas molecules, there are only a few reports on the epitaxial growth of uniform and smooth Pt_{ML} shell on core nanoparticles by solution-phase syntheses.[25,26]

Aerobic alcohol oxidation catalyzed heterogeneously by metal catalysts has been extensively investigated for the synthesis of valuable chemical precursors and intermediates.[27,28] Herein, we demonstrate that the ethanol oxidation catalyzed by metal nanoparticles can be employed for the epitaxial growth of Pt_{ML} on the metal particles. Ethanol, a nontoxic liquid that can be produced from renewable sources,[29] was employed as both reducing agent and solvent in the syntheses. We have recently demonstrated the successful syntheses of highly ordered Ru−Pt core−shell nanoparticles using the ethanol-based approach.[30] In a typical synthetic procedure, ethanol oxidation was catalyzed by the core nanoparticles and consequently generated electrons. These electrons were then utilized in the reduction of $[PtCl_6]^{2-}$ ions to Pt atoms, which were coated on core nanoparticles, forming atomic Pt layers. The reducing power of ethanol was tunable by adjusting temperature, H_2O, and pH (Supporting Information Figure S1). The reaction temperature was optimized (vide infra); water and base were added to provide hydroxide ions that were critical during aerobic alcohol oxidation by facilitating several elementary steps.[31] The simplicity of the ethanol-based synthetic approach allows for high scalability and reproducibility.

Carbon-supported palladium (Pd) nanoparticle was employed as the representative core to support the Pt_{ML} shell in this work because, among all noble metals, Pd was found to be the most appropriate substrate for Pt_{ML} toward the ORR.[32] After the Pt coating process, such Pd@Pt core−shell nanoparticles were observed to be evenly dispersed on the carbon support, shown by the transmission electron microscopy (TEM) image (Figure 1a). Their crystal structure is confirmed to be face-centered cubic (fcc, space group $Fm\bar{3}m$) by X-ray diffraction (XRD) (Figure 1b) and by selected-area electron diffraction (SAED) (Figure 1c). The similar crystal structure (fcc), and the small lattice mismatch (0.85%) between Pt (0.39236 nm) and Pd (0.38903 nm)[33] are beneficial for Pt to coherently match the lattice structure of Pd core and to form a pseudomorphic shell.[34]

Received: November 20, 2013
Revised: January 14, 2014
Published: January 16, 2014

   dx.doi.org/10.1021/cs401091u | *ACS Catal.* 2014, 4, 738−742

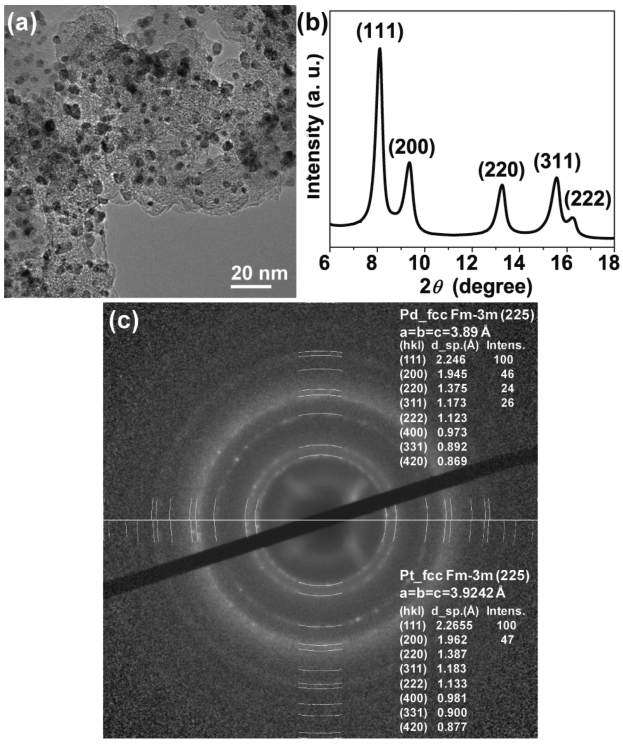

Figure 1. Morphology and crystal structure of Pd@Pt_{ML} sample. (a) TEM image in which the average size is 3.73 nm, (b) Synchrotron XRD (λ = 0.3196 Å) diffractogram. (c) Selected-area electron diffraction (SAED) equipped on a TEM, superimposed with the standard profiles of diffraction rings for Pd (top) and Pt (bottom).

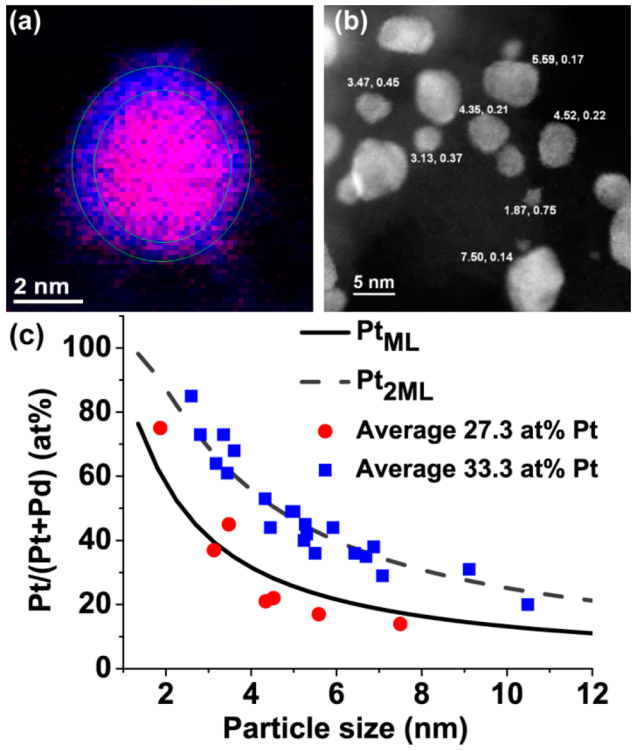

Figure 2. (a) STEM-HADDF image (blue) overlapping Pd EELS signal (red) for a representative Pd@Pt core−shell nanoparticle. (b) Representative HADDF image of Pd@Pt_{ML} nanoparticles. Individual particles are marked by (s, r) where s is the particle size and r is the Pt/(Pt + Pd) atomic ratio determined by EDX equipped on a STEM. (c) The EDX-determined Pt/(Pt + Pd) atomic ratio as a function of particle size for two distinct samples. The data for the Pt_{ML} sample (red dots) were measured from the area shown in part b, and the $Pt_{2\ ML}$ data (blue squares) were from Supporting Information Figure S2. The lines are the calculated curves for Pt_{ML} (solid) and $Pt_{2\ ML}$ (dashed) on Pd nanoparticles. Representative STEM−HAADF images for these two samples are shown in Supporting Information Figures S3 and S4.

The exclusive deposition of Pt atoms on Pd cores is verified by the two-dimensional (2D) intensity mapping (Figure 2a) of high-angle annular dark field (HAADF) image (blue) with electron energy-loss spectroscopy (EELS) signal of Pd (red) using scanning transmission electron microscopy (STEM) technique. In addition, the Pt/(Pt + Pd) atomic ratios were determined by energy dispersive X-ray spectroscopy (EDX) equipped on the STEM for individual particles (Figure 2b). No particles were found without the existence of Pd, indicating that the self-nucleation of Pt has been effectively inhibited. For two distinct samples (red dots and blue squares in Figure 2c) with different amounts of H_2PtCl_6 precursor in the syntheses, the measured Pt/(Pt + Pd) atomic ratios decrease with the increasing particle sizes. The trend primarily follows the curves calculated for Pt monolayer (Pt_{ML}) and bilayer (Pt_{2ML}) shells on Pd cores, respectively (solid and dashed lines in Figure 2c). The calculation was based on a cuboctahedron model and a normal distribution of particle size (see experimental details, Supporting Information). These results denote that simply increasing the amount of H_2PtCl_6 precursor could correspondingly increase the thickness of conformal Pt shells.

The uniform coating of Pt shells is partly attributed to the optimal reaction temperature of 70 °C, which has been chosen considering three aspects: First, in 1−5 mM ethanolic H_2PtCl_6 solutions, Pt nucleation did not occur until the solution temperature was higher than 78 °C, which is also the boiling point of ethanol. Second, the reducing power of ethanol at 70 °C was sufficient to reduce Pt(IV) to Pt(0) in the presence of Pd nanoparticles. The complete reduction of $[PtCl_6]^{2-}$ is signaled by the color of H_2PtCl_6 solution fading from pristine yellow to colorless during the coating process. The nearly 100% yield is also verified by the good agreement between metal compositions in final products measured by inductively coupled plasma mass spectrometry (ICP−MS) and by EDX equipped on a scanning electron microscope (SEM), with those calculated from the precursor amounts used in syntheses (Supporting Information Table S1). Third, at 70 °C, the reduction of Pt ions was dominated by the oxidation of ethanol rather than the oxidation of Pd atoms. Without a reducing agent, Pt atoms can be deposited via the galvanic displacement of Pd because Pd has a lower reduction potential than Pt.[35−37] That process could lead to either a small loss of Pd if the Pd ions remained in the solution at the end of synthesis or a Pd−Pt partially alloyed shell if oxidized Pd was reduced back by ethanol.

To better understand the growth mode of the Pt_{ML} shell on Pd nanoparticles at atomic level, we performed density functional theory (DFT) calculations. A hemisphere-like Pd_{174} nanoparticle model (Supporting Information Figure S6) was employed to represent a ∼2.2 nm spherelike truncated octahedral Pd_{405} nanoparticle (Figure 3a) containing {111} and {100} facets, which are typical exposing facets for small fcc metal nanoparticles.[38−40] Our previous studies demonstrated the capability of such a hemisphere model to well interpret the experimental electrochemical activities of core−shell nano-

dx.doi.org/10.1021/cs401091u | ACS Catal. 2014, 4, 738−742

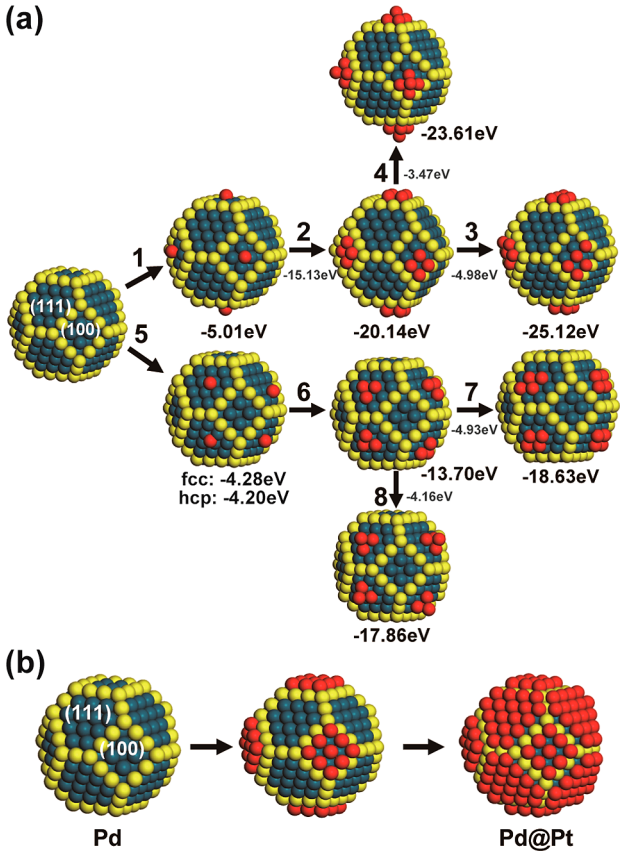

Figure 3. (a) DFT-calculated binding energies of Pt atoms (red) on {100} and {111} terraces of a Pd nanoparticle represented by a spherelike truncated octahedron Pd_{405} NP model with a 2.2 nm diameter. BEs are shown in electronvolts per facet. (b) Proposed growth scheme for spherelike truncated octahedral Pd@Pt core−shell NPs, based on the calculated BEs shown in part a. Color scheme: Dark blue for Pd atoms on terraces, yellow for Pd atoms at edges and vertices, and red for Pt atoms.

particles.[14,41] We first calculated the binding energy (BE) of a single Pt atom adsorbed at different sites of the Pd nanoparticle to understand nucleation at the very early stage of Pt growth. The lower the BE is, the more preferable is the site. The results exhibit that a Pt atom prefers the 4-fold hollow site on Pd {100} facets (BE = −5.01 eV, step 1 in Figure 3a), followed by the 3-fold hollow site on Pd {111} facets (−4.28 eV at an fcc site, −4.20 eV at an hcp site, step 5 in Figure 3a); then the bridge site at {111}/{111} edges (−3.75 eV); and, last, the bridge site at {100}/{111} edges (−3.04 eV). In addition, a Pt adatom at the vertex site spontaneously moves to the {111}/{111} edge site during the geometry optimization. Therefore, the deposited Pt atom is likely to nucleate on the {100} or {111} terraces (steps 1 and 5 in Figure 3a) rather than at edges (not shown).

Next, we studied the Pt growth mode after initial nucleation by comparing the BEs of Pt adatoms forming small Pt clusters on the {100} or {111} facets of Pd nanoparticle. A Pt_4 planar was employed to model the ordered Pt structure formed on Pd {100} facets, wherein each Pt atom sat at the most stable 4-fold hollow site. The Pt growth on Pd from an adatom to a 2D tetramer is highly exothermic, releasing an energy of −15.13 eV (step 2 in Figure 3a), suggesting that the 2D growth of Pt on Pd {100} is energetically preferred. It also shows that the further growth from Pt_4 to Pt_5 favors the formation of a 2D planar rather than a 3D cluster by 1.51 eV (steps 3 vs 4 in Figure 3a) because of the formation of additional strong Pt−Pt and Pt−Pd bonds. Similar phenomena were observed for Pd {111} facets as well (steps 6, 7, and 8 in Figure 3a), although energetically, the Pt growth on Pd {111} is less preferential than that on {100} facets (steps 7 vs 3 in Figure 3a).

Considering all the DFT results discussed above, we propose a growth scheme for the sphere-like truncated octahedral Pd@Pt core−shell nanoparticles (Figure 3b). The growth of the Pt shell starts from the formation of an ordered Pt monolayer on Pd {100} facets, followed by the closure of an ordered Pt monolayer on Pd {111}. A similar growth mode has been proposed recently for a ∼1.7 nm Pt@Cu core−shell nanoparticle.[42] Overall, our DFT-calculated results clearly demonstrate that the epitaxial layer-by-layer growth of Pt is thermodynamically favorable on Pd nanoparticles, and hence, the elevated temperature during syntheses should facilitate the formation of a smooth and uniform Pt shell on Pd cores.

The conformal and smooth Pt shell is further deduced from the electrochemical performances for $Pd@Pt_{ML}$ nanocatalysts. Table 1 summarizes the ORR activities for $Pd@Pt_{ML}$ and Pd@$Pt_{2\ ML}$ samples fabricated via the ethanol-based approach, compared with those for $Pd@Pt_{ML}$ prepared by the scale-up Cu UPD method. The smooth Pt surface formed at 70 °C by ethanol led to a smaller electrochemical surface area (ECSA) than that formed at room temperature by the scale-up Cu UPD method,[43] given that high-coordination sites on smooth terraces are less reactive to H adsorption/desorption than low-coordination sites on a roughened surface with edges and defects.[44−48] $Pd@Pt_{ML}$ samples fabricated by two distinct methods exhibit similar mass activities (normalized by Pt or PGM mass), indicating that the ethanol-based approach is an effective scale-up synthetic route to fabrications of Pt_{ML} catalysts.

Table 1. Mass Activities (MA) and Specific Activities (SA) for Pt_{ML} Samples Prepared by Ethanol-Based Approach or by Scale-Up Cu UPD, Derived from the ORR Kinetic Currents at 0.9 V (vs RHE)

	$Pd@Pt_{ML}$ Cu UPD	$Pd@Pt_{ML}$ ethanol	$Pd@Pt_{2ML}$ ethanol
Pt/(Pt + Pd) (at. %)	26.9	27.3	33.3
Pt (wt %)	16.5	17.1	18.1
Pd (wt %)	24.5	24.9	19.7
MA_{Pt} (A mg^{-1})[a]	0.62	0.64	0.62
MA_{PGM} (A mg^{-1})[b]	0.25	0.26	0.30
SA (mA cm^{-2})[c]	0.32	0.58	0.70
ECSA (m^2 g^{-1})[d]	191	110	89

[a]MA_{Pt}, mass activity normalized by the mass of Pt. [b]MA_{PGM}, mass activity normalized by the mass of Pt-group metals (PGM). [c]SA, specific activity normalized by the ECSA. [d]ECSA, electrochemical surface area.

Pt monolayer on Pd {111}. A similar growth mode has been proposed recently for a ∼1.7 nm Pt@Cu core−shell nanoparticle.[42] Overall, our DFT-calculated results clearly demonstrate that the epitaxial layer-by-layer growth of Pt is thermodynamically favorable on Pd nanoparticles, and hence, the elevated temperature during syntheses should facilitate the formation of a smooth and uniform Pt shell on Pd cores.

The conformal and smooth Pt shell is further deduced from the electrochemical performances for $Pd@Pt_{ML}$ nanocatalysts. Table 1 summarizes the ORR activities for $Pd@Pt_{ML}$ and Pd@$Pt_{2\ ML}$ samples fabricated via the ethanol-based approach, compared with those for $Pd@Pt_{ML}$ prepared by the scale-up Cu UPD method. The smooth Pt surface formed at 70 °C by ethanol led to a smaller electrochemical surface area (ECSA) than that formed at room temperature by the scale-up Cu UPD method,[43] given that high-coordination sites on smooth terraces are less reactive to H adsorption/desorption than low-coordination sites on a roughened surface with edges and defects.[44−48] $Pd@Pt_{ML}$ samples fabricated by two distinct methods exhibit similar mass activities (normalized by Pt or PGM mass), indicating that the ethanol-based approach is an effective scale-up synthetic route to fabrications of Pt_{ML} catalysts.

In addition to good catalytic activities, the $Pd@Pt_{ML}$ sample also exhibited exceptional durability after the pulse-potential stability test. As shown in Figure 4, after 5000 cycles of potential pulses (10 s at 0.6 V and at 1.0 V each, as shown in Supporting Information Figure S7), the ORR polarization curve remained unchanged, and the cyclic voltammetry curve showed negligible loss of ECSA. Previous studies found that the Pt_{ML} shell supported on treated Pd nanoparticles smoothed by Br adsorption provided higher stability than the Pt_{ML} shell

dx.doi.org/10.1021/cs401091u | ACS Catal. 2014, 4, 738−742

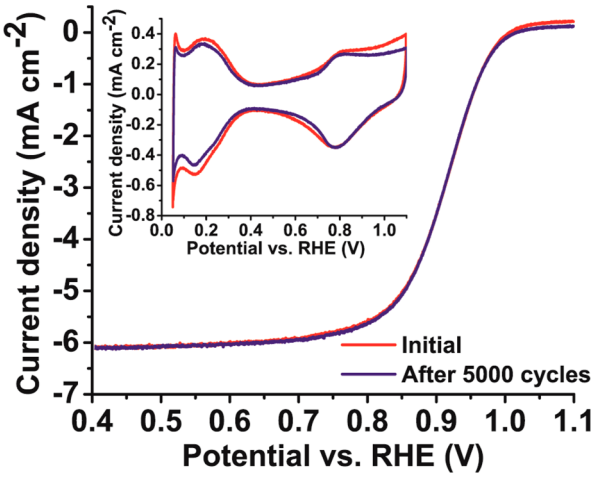

Figure 4. ORR polarization (10 mV s^{-1}, 1600 rpm) and cyclic voltammetry (inset) curves (50 mV s^{-1}) obtained in 0.1 M $HClO_4$ solutions on a $Pd@Pt_{ML}$ sample prepared by the ethanol-based approach before (red) and after (blue) 5000 potential-pulse cycles of 0.6 V (10 s) to 1.0 V (10 s) (Supporting Information Figure S7). Loading: 8.75 $\mu g\ cm^{-2}$ Pt, 12.74 $\mu g\ cm^{-2}$ Pd.

supported on untreated commercial Pd nanoparticles,[49] since the low-coordination sites at edges and defects are prone to dissolution.[50−52] Therefore, the excellent durability is attributed to the smooth surface morphology and complete Pt_{ML} shell.

In conclusion, we have demonstrated a surfactant-free and high-yield chemical route for coating of Pt atomic layers on Pd nanoparticles, which ensures high reproducibility and scalability. The conformity and continuousness of Pt shells were verified by various characterization techniques. Our DFT calculations also showed that two-dimensional growth is energetically favorable. The uniform and complete Pt coating is promoted by the coating process with slower kinetics and the reaction temperature of 70 °C rather than room temperature, compared with the galvanic displacement of underpotentially deposited Cu monolayer. The strategy illustrated here could be applicable to the fabrication of other bimetallic or multimetallic core−shell nanoparticles for various applications.

■ ASSOCIATED CONTENT

Ⓢ Supporting Information

Detailed experimental procedures, Figures S1−S8, and Table S1 are included. This material is available free of charge via the Internet at http://pubs.acs.org.

■ AUTHOR INFORMATION

Corresponding Authors

*E-mail: jia@bnl.gov.

*E-mail: adzic@bnl.gov

Present Address

⊥(R.S.) Shanghai Institute of Applied Physics, Chinese Academy Sciences Shanghai Synchrotron Radiation Facility, 239 Zhangheng Road, Pudong District, Shanghai 201204, China.

Notes

The authors declare no competing financial interest.

■ ACKNOWLEDGMENTS

This research was performed at Brookhaven National Laboratory (BNL) under Contract DE-AC02-98CH10886 with the U.S. Department of Energy (DOE). The DFT calculations were performed using computational resources at the Center for Functional Nanomaterials of BNL, and at the National Energy Research Scientific Computing Center (NERSC), which is supported by the Office of Science of the U.S. DOE under Contract No. DE-AC02-05CH11231.

■ REFERENCES

(1) Renner, H.; Schlamp, G.; Kleinwächter, I.; Drost, E.; Lüschow, H. M.; Tews, P.; Panster, P.; Diehl, M.; Lang, J.; Kreuzer, T.; Knödler, A.; Starz, K. A.; Dermann, K.; Rothaut, J.; Drieselmann, R.; Peter, C.; Schiele, R. In *Ullmann's Encyclopedia of Industrial Chemistry*; Wiley-VCH Verlag GmbH & Co. KGaA: Weinheim, 2000.
(2) Marković, N. M.; Ross, P. N., Jr. *Surf. Sci. Rep.* **2002**, *45*, 117−229.
(3) Solla-Gullon, J.; Vidal-Iglesias, F. J.; Feliu, J. M. *Annu. Rep. Prog. Chem., Sect. C: Phys. Chem.* **2011**, *107*, 263−297.
(4) Gasteiger, H. A.; Kocha, S. S.; Sompalli, B.; Wagner, F. T. *Appl. Catal., B* **2005**, *56*, 9−35.
(5) Debe, M. K. *Nature* **2012**, *486*, 43−51.
(6) Stephens, I. E. L.; Bondarenko, A. S.; Gronbjerg, U.; Rossmeisl, J.; Chorkendorff, I. *Energy Environ. Sci.* **2012**, *5*, 6744−6762.
(7) Yang, H. *Angew. Chem., Int. Ed.* **2011**, *50*, 2674−2676.
(8) Oezaslan, M.; Hasché, F.; Strasser, P. *J. Phys. Chem. Lett.* **2013**, *4*, 3273−3291.
(9) Adzic, R. R.; Zhang, J.; Sasaki, K.; Vukmirovic, M. B.; Shao, M.; Wang, J. X.; Nilekar, A. U.; Mavrikakis, M.; Valerio, J. A.; Uribe, F. *Top. Catal.* **2007**, *46*, 249−262.
(10) Adzic, R. *Electrocatalysis* **2012**, *3*, 163−169.
(11) Calle-Vallejo, F.; Koper, M. T. M.; Bandarenka, A. S. *Chem. Soc. Rev.* **2013**, *42*, 5210−5230.
(12) Brankovic, S. R.; Wang, J. X.; Adzic, R. R. *Surf. Sci.* **2001**, *474*, L173−L179.
(13) Zhang, J.; Mo, Y.; Vukmirovic, M. B.; Klie, R.; Sasaki, K.; Adzic, R. R. *J. Phys. Chem. B* **2004**, *108*, 10955−10964.
(14) Wang, J. X.; Inada, H.; Wu, L. J.; Zhu, Y. M.; Choi, Y. M.; Liu, P.; Zhou, W. P.; Adzic, R. R. *J. Am. Chem. Soc.* **2009**, *131*, 17298−17302.
(15) Jin, Y.; Shen, Y.; Dong, S. *J. Phys. Chem. B* **2004**, *108*, 8142−8147.
(16) Herrero, E.; Buller, L. J.; Abruña, H. D. *Chem. Rev.* **2001**, *101*, 1897−1930.
(17) Fayette, M.; Liu, Y.; Bertrand, D.; Nutariya, J.; Vasiljevic, N.; Dimitrov, N. *Langmuir* **2011**, *27*, 5650−5658.
(18) Jayaraju, N.; Vairavapandian, D.; Kim, Y. G.; Banga, D.; Stickney, J. L. *J. Electrochem. Soc.* **2012**, *159*, D616−D622.
(19) Nutariya, J.; Fayette, M.; Dimitrov, N.; Vasiljevic, N. *Electrochim. Acta* **2013**, *112*, 813−823.
(20) Liu, Y.; Gokcen, D.; Bertocci, U.; Moffat, T. P. *Science* **2012**, *338*, 1327−1330.
(21) Wang, Y.; Toshima, N. *J. Phys. Chem. B* **1997**, *101*, 5301−5306.
(22) Zolfaghari, A.; Conway, B. E. *J. Electroanal. Chem.* **2000**, *488*, 151−153.
(23) Brimaud, S.; Behm, R. J. *J. Am. Chem. Soc.* **2013**, *135*, 11716−11719.
(24) Taufany, F.; Pan, C.-J.; Rick, J.; Chou, H.-L.; Tsai, M.-C.; Hwang, B.-J.; Liu, D.-G.; Lee, J.-F.; Tang, M.-T.; Lee, Y.-C.; Chen, C.-I. *ACS Nano* **2011**, *5*, 9370−9381.
(25) Lim, B.; Wang, J. G.; Camargo, P. H. C.; Jiang, M. J.; Kim, M. J.; Xia, Y. N. *Nano Lett.* **2008**, *8*, 2535−2540.
(26) Jiang, M.; Lim, B.; Tao, J.; Camargo, P. H. C.; Ma, C.; Zhu, Y.; Xia, Y. *Nanoscale* **2010**, *2*, 2406−2411.
(27) Davis, S. E.; Ide, M. S.; Davis, R. J. *Green Chem.* **2013**, *15*, 17−45.
(28) Mallat, T.; Baiker, A. *Chem. Rev.* **2004**, *104*, 3037−3058.
(29) Li, M.; Kowal, A.; Sasaki, K.; Marinkovic, N.; Su, D.; Korach, E.; Liu, P.; Adzic, R. R. *Electrochim. Acta* **2010**, *55*, 4331−4338.

(30) Hsieh, Y.-C.; Zhang, Y.; Su, D.; Volkov, V.; Si, R.; Wu, L.; Zhu, Y.; An, W.; Liu, P.; He, P.; Ye, S.; Adzic, R. R.; Wang, J. X. *Nat. Commun.* **2013**, *4*, 2466.
(31) Zope, B. N.; Hibbitts, D. D.; Neurock, M.; Davis, R. J. *Science* **2010**, *330*, 74−78.
(32) Zhang, J. L.; Vukmirovic, M. B.; Xu, Y.; Mavrikakis, M.; Adzic, R. R. *Angew. Chem. Int. Ed.* **2005**, *44*, 2132−2135.
(33) Haynes, W. M., Lide, D. R., Eds. *CRC Handbook of Chemistry and Physics*, 94th (Internet Version) ed.; CRC Press/Taylor and Francis: Boca Raton, FL, 2014.
(34) Sanchez, S. I.; Small, M. W.; Zuo, J.-m.; Nuzzo, R. G. *J. Am. Chem. Soc.* **2009**, *131*, 8683−8689.
(35) Hong, J. W.; Kang, S. W.; Choi, B.-S.; Kim, D.; Lee, S. B.; Han, S. W. *ACS Nano* **2012**, *6*, 2410−2419.
(36) Zhang, H.; Jin, M.; Wang, J.; Li, W.; Camargo, P. H. C.; Kim, M. J.; Yang, D.; Xie, Z.; Xia, Y. *J. Am. Chem. Soc.* **2011**, *133*, 6078−6089.
(37) Alia, S. M.; Jensen, K. O.; Pivovar, B. S.; Yan, Y. *ACS Catal.* **2012**, *2*, 858−863.
(38) Lim, B.; Jiang, M. J.; Camargo, P. H. C.; Cho, E. C.; Tao, J.; Lu, X. M.; Zhu, Y. M.; Xia, Y. N. *Science* **2009**, *324*, 1302−1305.
(39) Tao, A. R.; Habas, S.; Yang, P. *Small* **2008**, *4*, 310−325.
(40) Shao, M.; Peles, A.; Shoemaker, K. *Nano Lett.* **2011**, *11*, 3714−3719.
(41) Wang, J. X.; Ma, C.; Choi, Y.; Su, D.; Zhu, Y.; Liu, P.; Si, R.; Vukmirovic, M. B.; Zhang, Y.; Adzic, R. R. *J. Am. Chem. Soc.* **2011**, *133*, 13551−13557.
(42) Carino, E. V.; Kim, H. Y.; Henkelman, G.; Crooks, R. M. *J. Am. Chem. Soc.* **2012**, *134*, 4153−4162.
(43) Sasaki, K.; Wang, J. X.; Naohara, H.; Marinkovic, N.; More, K.; Inada, H.; Adzic, R. R. *Electrochim. Acta* **2010**, *55*, 2645−2652.
(44) Zhang, Y.; Ma, C.; Zhu, Y.; Si, R.; Cai, Y.; Wang, J. X.; Adzic, R. R. *Catal. Today* **2013**, *202*, 50−54.
(45) Wang, D.; Xin, H. L.; Yu, Y.; Wang, H.; Rus, E.; Muller, D. A.; Abruña, H. D. *J. Am. Chem. Soc.* **2010**, *132*, 17664−17666.
(46) Koenigsmann, C.; Zhou, W. P.; Adzic, R. R.; Sutter, E.; Wong, S. S. *Nano Lett.* **2010**, *10*, 2806−2811.
(47) Stamenkovic, V. R.; Mun, B. S.; Arenz, M.; Mayrhofer, K. J. J.; Lucas, C. A.; Wang, G.; Ross, P. N.; Markovic, N. M. *Nat. Mater.* **2007**, *6*, 241−247.
(48) Spendelow, J. S.; Xu, Q.; Goodpaster, J. D.; Kenis, P. J. A.; Wieckowski, A. *J. Electrochem. Soc.* **2007**, *154*, F238−F242.
(49) Cai, Y.; Ma, C.; Zhu, Y.; Wang, J. X.; Adzic, R. R. *Langmuir* **2011**, *27*, 8540−8547.
(50) Rinaldo, S. G.; Stumper, J. r.; Eikerling, M. *J. Phys. Chem. C* **2010**, *114*, 5773−5785.
(51) Komanicky, V.; Chang, K. C.; Menzel, A.; Markovic, N. M.; You, H.; Wang, X.; Myers, D. *J. Electrochem. Soc.* **2006**, *153*, B446−B451.
(52) Sheng, W.; Chen, S.; Vescovo, E.; Shao-Horn, Y. *J. Electrochem. Soc.* **2012**, *159*, B96−B103.